Design of a foil-coiled inductor for the heating of steel wires

J. De Coster, G. Deliège, F. Henrotte, U. Pahner, J. Fransen, D. Van Dommelen and K. Hameyer

Abstract: The main advantage of induction heating over other electroheating methods resides in its speed and efficiency of heating. In some cases, however, practical constraints can make high efficiencies hard to obtain by using classical solenoid inductors. Therefore, the design of a foil-coiled inductor as a possible alternative for classical coils is presented. This inductor consists of a wide thin copper sheet that is coiled around an insulating central tube. When studying classical induction coils, it is sufficient to consider only one turn. This leads to relatively small finite element models. A similar approach is not possible in the case of the foil-coiled inductor. To avoid very large models, the foil-coiled inductor has been studied by using two small and complementary models. One of these represents the end part of the inductor; the other one represents the middle section. Both non-linear time-harmonic electromagnetic calculations and coupled thermal-electromagnetic calculations have been performed on these models. The results of these calculations allowed a prototype coil to be constructed and measurements were carried out on an experimental set-up. The match between calculations and measurements was satisfactory.

1 Introduction

The main advantage of induction heating over other electroheating methods resides in its speed and efficiency of heating. In some cases, however, practical constraints can make a high efficiency hard to obtain by using classical solenoid inductors [1]. As a consequence, the performance of other inductor geometries should be studied. This paper deals with the design of a foil-coiled inductor as an alternative for classical solenoid coils.

2 The foil-coiled inductor concept

The foil-coiled inductor consists of a wide, thin copper sheet, coiled around an insulating central tube. An air gap is left between two consecutive layers to allow cooling. The electrical connection of the inner layer is realised through a copper bar that is placed parallel to the insulating tube. The steel wire to be heated travels along the central tube. An inductor of this kind is shown in Fig. 1.

3 Modelling of the inductor

When modelling an induction heating system with a classical solenoidal inductor, it may be sufficient in some cases to consider only one turn of the coil [2]. The system can then be studied by using relatively small numerical models. In the case of the foil-coiled inductor, the entire inductor has to be considered in the model. This leads to considerably larger models, which cannot be handled easily. Therefore, the following approach has been used.

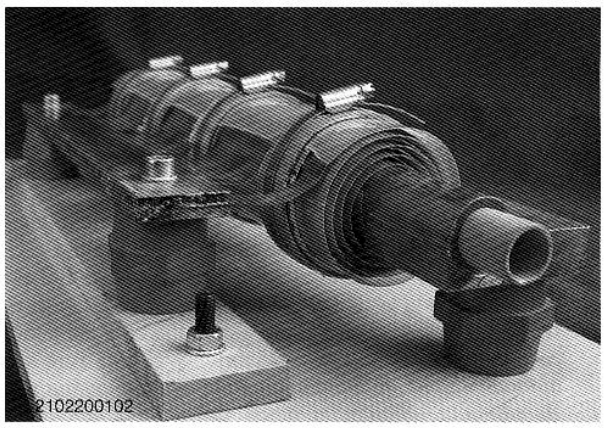

Fig. 1 *Photograph of the foil-coiled inductor*

3.1 Problem formulation for electromagnetic calculations

As a first stage, material properties were considered to be temperature-independent and a non-linear magnetic characteristic was assumed for the steel wire. A time-harmonic, non-linear calculation was performed to solve (1) [3] for the axisymmetric problem by the finite element method:

$$-\frac{\partial}{\partial r}\left(\nu\frac{\partial(rA_\theta)}{r\,\partial r}\right)-\frac{\partial}{\partial x}\left(\nu\frac{\partial A_\theta}{\partial x}\right)+j\omega\sigma A_\theta=-\sigma\Delta V \quad (1)$$

where r and x are the radial and axial co-ordinates respectively, A_θ is the tangential component of the magnetic vector potential, ν is the magnetic reluctivity and σ is the material's conductivity. The magnetic vector potential has to be calculated from the given applied voltage. The motion term may be omitted, since the velocity-induced magnetic field is negligible with respect to the main field in this

IEE Proceedings online no. 20020566

DOI: 10.1049/ip-smt:20020566

Paper first received 13th March 2002 and in revised form 10th June 2002

J. De Coster, G. Deliège, F. Henrotte, U. Pahner, D. Van Dommelen and K. Hameyer are with the Department of EE (ESAT)/Division ELECTA, Katholieke Universiteit Leuven, Kasteelpark Arenberg 10, Leuven B-3001, Belgium

J. Fransen is with the Bekaert Technology Centre, Bekaertstraat 2, Zwevegem B-8550, Belgium

application [2]. As a consequence, the magnetic field is symmetric along the axis of the inductor and it is therefore sufficient to model one-half of it. The following analytic formula was used [2] to represent the non-linear magnetic characteristic of steel:

$$\begin{aligned} \nu(B) &= \frac{\nu_0}{\mu_r} \quad B \le B_l \\ &= \frac{\nu_0}{\mu_r} 10^{\alpha(B-B_l)} \quad B \le B_n \\ &= \frac{H_n + \nu_0(B - B_n)}{B} \quad B > B_n \end{aligned} \tag{2}$$

An approximated phasor approach was used to allow performing time-harmonic calculations with the non-linear material [4]. This method consists in substituting the magnetic reluctivity from (2) in the constitutive law $H = \nu B$ with an equivalent complex reluctivity, forcing thus both H and B to be sinusoidal. The value of this equivalent reluctivity is determined so as to obtain an equal reversible magnetic energy exchange and equal hysteretic losses in the model and in the actual material. This allows using the computationally efficient phasor representation, despite the presence of non-linear materials in the problem.

To solve the model of the foil-coiled inductor, the GetDP-software package (general software environment for the treatment of discrete problems) was used [5]. The computed current density at the surface of the wire and in the coil is shown in Fig. 2. The x-axis is the axial co-ordinate as indicated in Fig. 3. The origin is located at one end of the inductor and the x-values are normalised with respect to the length of the inductor. The current density that is plotted on the vertical axis, is normalised with respect to the maximum current density that occurs in the inductor.

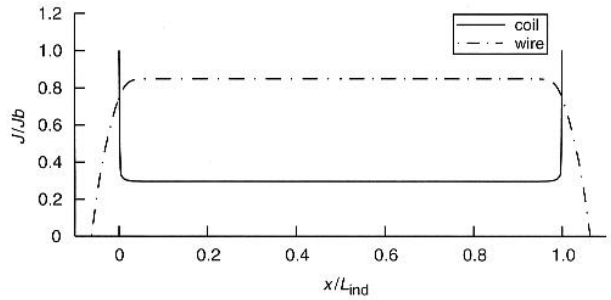

Fig. 2 *Current density in the wire and in the inductor (Axes are normalised with respect to the inductor length and the maximum current density)*

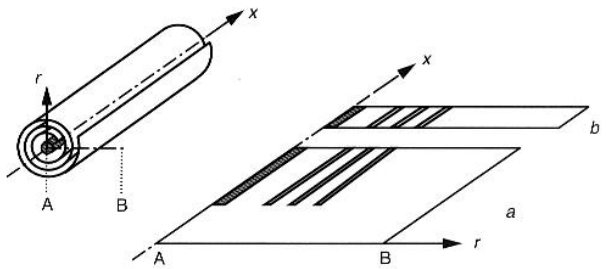

Fig. 3 *Two axisymmetric models of the foil-coiled inductor*

3.2 Choice of model geometry

Due to the skin effect, the current density in the inductor exhibits a large peak at both ends of the inductor. A similar effect is observed for the induced current in the wire. The moving wire leaves the inductor and therefore the mutual coupling wire/coil decreases rapidly and hence the current density drops to zero.

Despite these steep changes of amplitude, both current densities level out quickly towards the middle of the conductors. In order to represent the sharp variation of the current density at the endparts of the inductor, it is therefore sufficient to model only a limited part of the inductor length (about 10% in this case). This model is shown in Fig. 3*a*. In addition, a second model representing the middle section of the inductor was constructed (Fig. 3*b*) in order to verify whether the first model was sufficiently long or not, i.e. whether it extended far enough towards the region with a constant solution (cf. Fig. 2).

3.3 Meshing considerations

The operating frequency of induction heating equipment is usually chosen so as to maximise the wire diameter/skin depth ratio. In this case, the design frequency was fixed at 50 kHz, resulting in a diameter/skin depth ratio of about 30. Provided that the temperature remains below the Curie temperature (no demagnetisation), the large gradients of the electromagnetic phenomena (skin effect) will be located within a very thin layer under the surface of the wire. This makes it unnecessary to have a fine mesh in the centre of the wire, whereas a very fine mesh is required close to its surface.

A mesh that gradually refines as one approaches the surface of the wire is very suitable in this case (Fig. 4*a*). A similar mesh was used for the coil layers (Fig. 4*b*). The bold

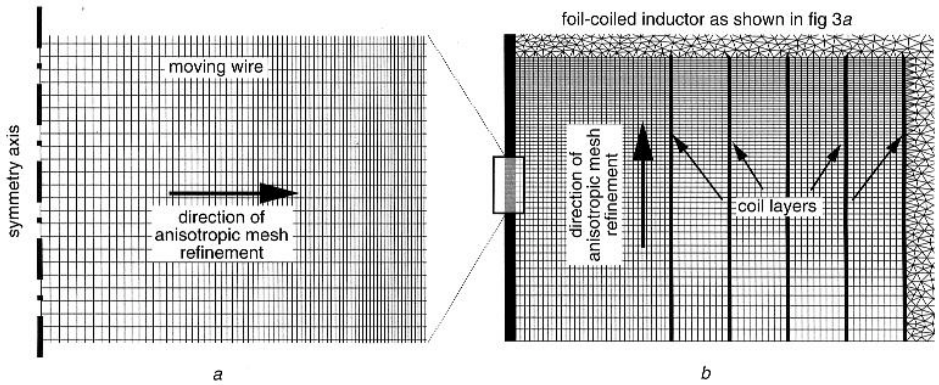

Fig. 4
a Gradually refining mesh in the wire
b Gradually refining mesh in the inductor
(The scale for the wire and the coil are not the same)

arrows in this figure indicate the direction of anisotropic mesh refinement.

4 Design parameters

4.1 Introduction

Since inductor efficiency is an important issue, the influence of several coil dimensions was examined. The efficiency is given by:

$$\eta = \frac{P_{\text{supply}} - P_{\text{coil}}}{P_{\text{supply}}} \tag{3}$$

with

$$P_{\text{coil}} = 2\pi\sigma_{\text{Cu}} \int\int |j\omega \boldsymbol{A} + \nabla \boldsymbol{V}|^2 r\, dr\, dx \tag{4}$$

As an example, Fig. 5 shows the influence of the inductor length and the applied voltage on efficiency. According to Fig. 2, one can conclude that the major contribution to the Joule losses in the inductor (P_{coil}) is due to the current density peaks at the end section of the inductor. When the inductor length increases, that contribution becomes relatively less important, increasing thereby the efficiency. Thus, in order to obtain a better efficiency, Fig. 5 shows it is favourable to use a long inductor and to supply it with a low voltage. The values on the 'voltage'-axis as well as on the 'length'-axis are expressed as multiples of a reference value.

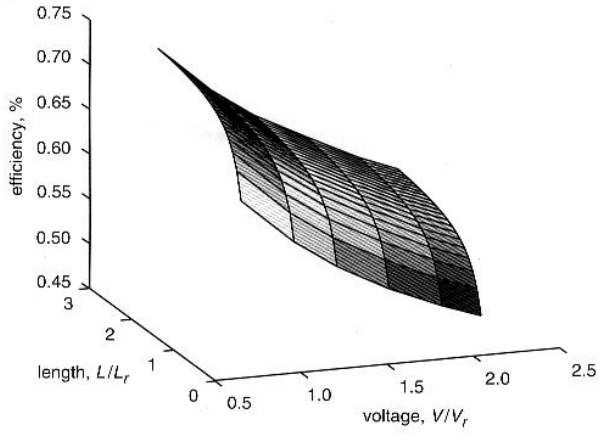

Fig. 5 *Influence of inductor length and applied voltage on efficiency (L_r and V_r are reference length and voltage respectively)*

4.2 Foil thickness

The thickness of the foil used for the construction of the inductor is another very important design parameter. Faraday's law

$$\nabla \times (\rho \boldsymbol{J}) = -j\omega \boldsymbol{B} \tag{5}$$

shows that there is a 90° phase shift between current density and magnetic induction. This phase shift exists for both the inductor current and the induced current in the wire. Since the inductor current supplies energy to the magnetic field and the current in the wire picks up energy from the field, the two currents are shifted by 180°.

Due to the self-inductance of the coil, a certain amount of current is also induced in the coil itself. Consequently, there exist two current components in the coil that are shifted by 180°. Of course this is true for all inductors, but in the case of a multi-layer coil, such as the foil-coiled inductor, this has a rather peculiar consequence.

The proximity effect causes the two current components to be spatially separated. The component that lags behind the supply voltage, flows near to the inner surface of each turn of the foil-coiled inductor, while the component that is 90° ahead, flows rather near the outer surface. This can be seen in Fig. 6, where the phase angle of the current density is given as a function of the radial co-ordinate inside the innermost coil layer.

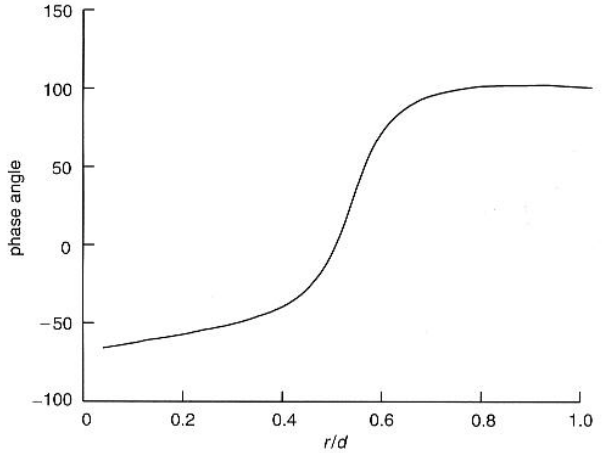

Fig. 6 *Phase angle distribution of the current density inside a coil layer (d is the thickness of the foil)*

When the thickness of the foil is decreased, both current components are forced into each other, causing them to partly cancel out. Therefore, the mean current density decreases with decreasing foil thickness, increasing thereby the efficiency. In order to obtain optimal inductor efficiency, the foil thickness should be reduced below the skin depth in the inductor material. For a frequency of 50 kHz, this means the foil should be at most 0.3 mm thick. The foil should not be made thinner either, for this causes the current density peak observed in Fig. 2 to increase. This may yield serious cooling problems.

The result shown in Fig. 6 has also an important consequence regarding the electromagnetic forces acting on the turns of the foil inductor. As there are two current components, shifted by 150°, there are two opposite force components also acting on the foil layer. This leads, however, to a much lower force density than the one that would be expected by only considering the absolute value of the current density. The force acting on the coil layers is given by:

$$\frac{F_r}{\Omega} = \int (\nabla \times \boldsymbol{A})_x (-j\omega\sigma_{\text{cu}} \boldsymbol{A} - \sigma_{\text{cu}} \nabla V)_\theta dr \tag{6}$$

where Ω is the surface area of the foil and where the integration is performed over the layer thickness, and the subscript θ denotes the tangential component. Calculations show that the density does not exceed a few tens of Pascals. Even though the foil is relatively thin, no mechanical problems are encountered. This was confirmed during tests on the prototype.

5 Coupled thermal-electromagnetic computation

In a second design stage, coupled thermal-electromagnetic calculations were performed, taking the temperature-dependency of the material properties of the wire (σ, ν, ρ and c) into account. Solving (6) in a reference frame that is fixed to the wire makes the motion term $-\rho c \boldsymbol{v} \cdot \nabla T$ vanish,

avoiding thus the numerical problems that would be encountered in the laboratory frame.

$$-\rho c\frac{dT}{dt} - \rho c\mathbf{v}\cdot\nabla T + \nabla\cdot(\lambda\nabla T) = -q \qquad (7)$$

This approach, however, is allowed only in case of an axial symmetry, i.e. the geometry of the inductor remains unchanged by translation along the x-axis. When using the model from Fig. 3*b*, this condition is clearly fulfilled. This means though that end-effects cannot be taken into account. The error caused by this approximation can be estimated by evaluation of (7) where P_{real} is evaluated for the mean wire temperature, and the integration is done over the whole length of the wire (this consists of twice the section from Fig. 3*a* plus $L_{3b}/(L_{wire}-2L_{3a})$ times the section from Fig. 3*b*). P_{simul} is the sum of the powers from all time steps. The error is of the order of a few percent.

$$\delta P = \frac{P_{simul} - P_{real}}{P_{real}} \qquad (8)$$

with

$$P_{real} = 2\pi\sigma_{Fe}\int\int |j\omega A|^2 r\,dr\,dx \qquad (9)$$

The system is solved using weak coupling, i.e. an electromagnetic and a thermal calculation are performed in each time step and the material properties are updated after each successive calculation according to the computed field values. Fig. 7 shows the temperature increase of the wire as it travels through the inductor.

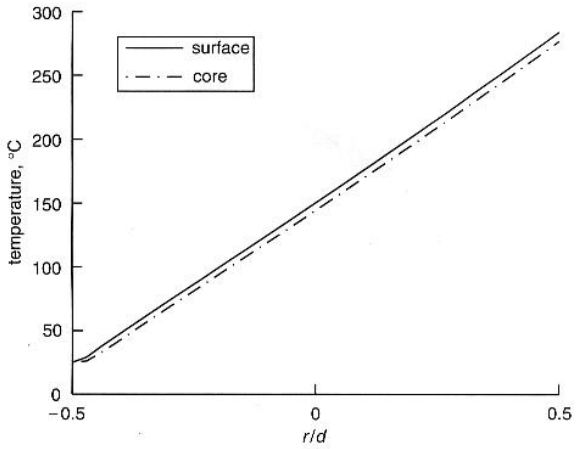

Fig. 7 *Temperature increase of the wire as it travels through the inductor*

6 Measurements

A prototype coil was built and tested on a wire treatment line. Since the foil-coiled inductor has only five turns, a large current is needed to attain a given magnetic field. As a consequence, bundles of copper strips are required for the electrical connections of the coil. Unfortunately, these exhibit a large inductance and a finite element model (FEM) model was created to calculate their impedance. The equivalent circuit of Fig. 8 is then obtained.

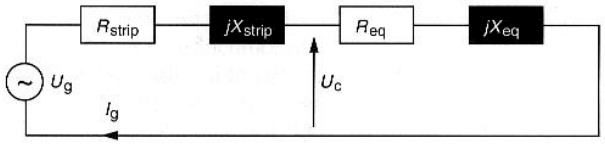

Fig. 8 *Equivalent circuit of the connected coil*

R_{eq} and X_{eq} are the equivalent parameters that represent the coil and the wire travelling through it. The values are extracted from an FEM solution. By means of this circuit, the voltage across the terminals of the coil and hence the power dissipated in the wire can be calculated when the generator voltage U_g is measured. In Fig. 9, a comparison is made between the measured values of the generator voltage U_g, the power delivered by the generator (P_g), the surface temperature of the wire when leaving the inductor (T_{out}) and their corresponding calculated values.

Measurements	equivalent circuit	Calculations
U_g = 244 V	→	I_g = 530 A
		P_{strips} = 1.26 kW
		P_{coil} = 767 W
P_{wire} = 530 W[(1)]		P_{wire} = 646 W
P_g = 3.00 kW		$P_g = \Sigma P_i$ = 2.68 kW
T_{out} = 341 °C		T_{out} = 394 °C

[(1)] derived from measured value of T_{out}

Fig. 9 *Comparison between measurements and calculations*

7 Conclusions

Foil-coiled inductors cannot be modelled in the same way as classical solenoidal inductors. For non-linear, time-harmonic electromagnetic calculations, end-effects can be considered accurately. Even though this is not possible for coupled thermal-electromagnetic calculations, the calculated results without end-effects have a satisfactory accuracy. In principle it is therefore sufficient to study the foil-coiled inductor by means of a small section in the middle of the coil. Attention has to be paid, however, to the large current density peak that appears at the edge of the inductor. This peak does not cause high electromagnetic forces, but it should be kept within limits to prevent excessive heating of the coil. A prototype coil has been built and results have been verified by measurements.

8 Acknowledgments

The authors are grateful to the Belgian 'Fonds voor Wetenschappelijk Onderzoek Vlaanderen' for its financial support of their work and the Belgian Ministry of Scientific Research for granting the IUAP P4/20 on Coupled Problems in Electromagnetic Systems. The research council of the K.U. Leuven supports the basic numerical research.

9 References

1 ORFEUIL, M.: 'Electric Process Heating', (Batelle Press, Columbus, OH, USA, 1987)
2 HENROTTE, F., DELIEGE, G., HAMEYER, K., and FRANSEN, J.: 'Finite Element Modelling of the induction heating of a moving wire'. 13th Conference on the Computation of electromagnetic fields, COMPUMAG 2001, Evian, France, July 2001, pp. 2–7
3 HAMEYER, K., and BELMANS, R.: 'Numerical Modelling and Design of Electrical Machines and Devices', (WIT Press, Southampton, UK, 1999)
4 HEDIA, H., HENROTTE, F., DULAR, P., GENON, A., and LEGROS, W.: 'Determination of equivalent material characteristics for parasitic effects in electrical apparatus', *IEEE Trans. Magn.*, 1996, **32**, (5), pp. 4341–4343
5 DULAR, P., GEUZAINE, C.: http://www.geuz.org/getdp